Marginal Instability and the Efficiency of Ocean Mixing

W. D. SMYTH

College of Earth, Ocean and Atmospheric Sciences, Oregon State University, Corvallis, Oregon

(Manuscript received 23 April 2020, in final form 4 June 2020)

ABSTRACT

The mixing efficiency of stratified turbulence in geophysical fluids has been the subject of considerable controversy. A simple parameterization, devised decades ago when empirical knowledge was scarce, has held up remarkably well. The parameterization rests on the assumption that the flux coefficient Γ has the uniform value 0.2. This note provides a physical explanation for $\Gamma = 0.2$ in terms of the "marginal instability" property of forced stratified shear flows, and also sketches a path toward improving on that simple picture by examining cases where it fails.

1. Introduction

A central goal of turbulence research is to predict fluxes of momentum, mass, and other scalars through a given turbulent flow. A simple and flexible approach to this problem is the flux-gradient formalism (Boussinesq 1903; Pope 2000), which requires the use of an effective (or "eddy") viscosity and corresponding diffusivities for mass and any other relevant scalars. An essential step toward prediction is to explore the variability of these quantities over the diverse turbulence regimes found in nature. Unfortunately these quantities are generally difficult to measure, so we must devise indirect methods. For the case of mass, the eddy diffusivity K_ρ can be written as

$$K_\rho = \Gamma \frac{\varepsilon}{N^2}, \tag{1}$$

where ε is the viscous dissipation rate of turbulent kinetic energy, N is the buoyancy frequency, and Γ is an unknown function, defined implicitly by (1), that we refer to as the *flux coefficient*. In the ocean, N and ε are measured routinely, so if the value of Γ is available, (1) yields K_ρ. One can then take advantage of the fact that different scalar concentrations diffuse at similar rates and therefore use K_ρ as an approximation for the diffusivity of heat, salt, CO_2, or any other scalar.

Eventually we hope to be able to calculate values of Γ for all the various processes that mix geophysical fluids. In the interim, we use the provisional value $\Gamma = 0.2$. This is an oversimplification, but when checked independently as described below, $\Gamma = 0.2$ gives accurate diffusivity estimates remarkably often. As emphasized in the recent review of Gregg et al. (2018), "The reasons for this agreement ... are not fully understood, nor are the circumstances under which it might fail." The dual purposes of this note are therefore (1) to propose an explanation for the prevalence of $\Gamma = 0.2$ and (2) to explore the boundaries of its validity.

a. Definitions

A quantity closely related to Γ is the mixing efficiency (Gregg et al. 2018). For any thermodynamic process, efficiency is the ratio of the work done to the energy input. We therefore define mixing efficiency in the context of the turbulent kinetic energy equation. Consider homogeneous turbulence in a sheared, stably stratified environment. Under the Boussinesq approximation, the evolution of the turbulent kinetic energy k is controlled by the sum of three processes:

$$\frac{dk}{dt} = K_m S^2 - K_\rho N^2 - \varepsilon. \tag{2}$$

The first term on the right-hand side, the product of the eddy viscosity K_m, and the squared shear of the mean horizontal velocity S^2, represents the input of kinetic energy to the turbulence from the mean current. The second term is the rate of working against gravity, and the third is the rate of viscous dissipation.

Denotes content that is immediately available upon publication as open access.

Corresponding author: W. D. Smyth, bill.smyth@oregonstate.edu

DOI: 10.1175/JPO-D-20-0083.1

On average, we can assume that the turbulence is in equilibrium with whatever is forcing it, so the time derivative in (2) vanishes and the remaining three terms balance. Rearranging, we can see this as a budget for the energy gained from the mean shear:

$$K_m S^2 = K_\rho N^2 + \varepsilon. \tag{3}$$

Some of this energy goes into work against gravity, and the rest is dissipated by viscosity (the first and second terms on the right-hand side, respectively). The flux coefficient Γ is the ratio of the rates of these two processes.

The mixing efficiency as defined above is the ratio of the first two terms on the right-hand side of (2): $(K_\rho N^2)/(K_m S^2)$. This is also called the flux Richardson number R_f, which can be written as the ratio of the gradient Richardson number, $\mathrm{Ri} = N^2/S^2$, to the turbulent Prandtl number $\mathrm{Pr}_t = K_m/K_\rho$:

$$R_f = \frac{\mathrm{Ri}}{\mathrm{Pr}_t}. \tag{4}$$

In equilibrium, when (3) holds, Γ and R_f are simply related:

$$\Gamma = \frac{R_f}{1 - R_f}. \tag{5}$$

Inasmuch as both Γ and R_f are generally much less than 1, they are nearly equal. In the literature one can find either R_f or Γ referred to as the "mixing efficiency," but only R_f is consistent with the standard thermodynamical definition.

b. History

In the initial theoretical estimate of R_f, Ellison (1957) noted that turbulence can do only a limited amount of work against gravity relative to its energy supply. After numerous assumptions, he proposed that turbulence could not be sustained unless $R_f < 0.15$. Arya (1972) later refined Ellison's assumptions and amended this estimate to 0.2. Laboratory measurements by Britter (1974) gave the range 0.18–0.2.

The default oceanic value $R_f = 0.17$, or $\Gamma = 0.2$, was first proposed by Osborn (1980) and is still in use today. Naturally, Osborn was aware that Γ varies but, lacking a way to predict the variations, he made the simplest assumption possible. Today, we seek to parameterize Γ in terms of other quantities that are readily measured observationally or computed in numerical models (e.g., Bouffard and Boegman 2013; Mashayek et al. 2017b). In this note I will lay out some physical considerations that may help to guide that effort.

The flux coefficient can be estimated from ocean microstructure measurements using the temperature variance equation for stationary, homogeneous turbulence (Osborn and Cox 1972; Oakey 1982), which results in

$$\Gamma \approx \frac{\chi}{2\varepsilon} \frac{N^2}{\Theta_z^2}, \tag{6}$$

where χ is the temperature variance dissipation rate and Θ_z is the vertical gradient of the mean potential temperature. This approximation assumes that K_ρ equals K_T, i.e., that heat and salt diffuse at the same rate. Estimates made in this way tend to agree with the Osborn's (1980) value to within a few tens of percent, a reasonable tolerance given the natural intermittency of turbulence and the difficulty of making delicate measurements in the ocean environment. Using (6) with profiler measurements made in the Rockall Trough, Oakey (1982, 1985) found a distribution of values with median $\Gamma = 0.26$ (or $R_f = 0.21$). Moum (1996) measured overturns in the thermocline off Northern California, and found a median Γ of 0.25 ($R_f = 0.20$). From profiler measurements in the North Atlantic, Ruddick et al. (1997) found a distribution of Γ with mean value 0.18. The logarithmic standard deviation was a factor of 2.6.

Independent confirmation of these estimates has come from a sequence of dye release experiments (Ledwell et al. 1998, 2000, 2004, 2011). Moreover, the moored microstructure instrument χ-pod measures χ and N^2 from temperature microstructure, then uses (6), together with an estimate for Γ, to infer ε. Perlin and Moum (2012) chose $\Gamma = 0.2$ and compared the results with measurements of ε from shear probes on an independent turbulence profiler. The comparison was good to within approximately a factor of 2, implying that $\Gamma = 0.2$ to within a similar tolerance.

The modern debate over mixing efficiency began with DNS studies of uniformly stratified shear flow (Shih et al. 2000, 2005; Ivey et al. 2008). Mixing efficiency was found to collapse when plotted as a function of the buoyancy Reynolds number, defined as $\mathrm{Re}_b = \varepsilon/(\nu N^2)$, where ν is the molecular viscosity. Specifically, mixing efficiency decreases like $\mathrm{Re}_b^{-1/2}$ at high Reynolds numbers, suggesting that $\Gamma = 0.2$ could be a serious overestimate in high-Re_b geophysical flows.

Since then, many investigators have made observations in energetic turbulence to try to understand the behavior of mixing efficiency at high Reynolds number. Results were reviewed by Monismith et al. (2018), who concluded that R_f (and hence Γ) cannot be determined by Re_b alone. However, it was also apparent that R_f (and hence Γ) often decreases in proportion to $\mathrm{Re}_b^{-1/2}$ at

TABLE 1. Estimates of Pr_t, R_f and Γ for Ri = 1/4.

Formula [also Eqs. (4) and (5)], reference	Pr_t	R_f	Γ
$R_f = 0.725(\mathrm{Ri} + 0.186 - \sqrt{\mathrm{Ri}^2 - 0.316\mathrm{Ri} + 0.0346})$ (Mellor and Yamada 1974)	1.19	0.21	0.27
$\mathrm{Pr}_t = 0.8 + 3.0\mathrm{Ri}$ (Esau and Grachev 2007)	1.55	0.16	0.19
$\mathrm{Pr}_t = 0.7e^{-3\mathrm{Ri}/0.7} + 4\mathrm{Ri}$ (Venayagamoorthy and Stretch 2010)	1.19	0.21	0.26
$R_f = \frac{1}{2} + 2\mathrm{Ri} - \sqrt{\frac{1}{4} + \mathrm{Ri} + 4\mathrm{Ri}^2}$ (Katul et al. 2014)	2.02	0.13	0.15

sufficiently high Re_b, consistent with the Shih et al. (2000, 2005) numerical results.

To summarize, despite strong suggestions that mixing efficiency decreases in energetic ocean flows, there remains considerable evidence in support of the approximation $\Gamma = 0.2$ ($R_f = 0.17$). In section 2, I will propose an explanation for this: geophysical turbulence is often in a state of *marginal instability* (hereafter MI), and MI implies $\Gamma \approx 0.2$. I will also discuss general conditions under which we might expect Γ to be far from 0.2 (section 3a) together with specific examples in which $\Gamma \gg 0.2$ (section 3b) and $\Gamma \ll 0.2$ (section 3c). The latter category includes cases in which $\Gamma \sim \mathrm{Re}_b^{-1/2}$. Section 4 summarizes the discussion and suggests directions for future work.

2. $\Gamma \approx 0.2$ in marginally unstable turbulence

An important mechanism of turbulence production in parallel shear flows is the inflectional instability, which operates at local maxima of the mean shear profile (Smyth and Carpenter 2019). Stable stratification tends to damp inflectional instability, but the instability may yet grow provided that the minimum of Ri is below a critical value. In this case the process is termed Kelvin–Helmholtz (KH) instability. In the inviscid limit, the critical Ri is 1/4 (Miles 1961; Howard 1961). The critical value may be altered by various factors including viscosity and diffusion (which may be either molecular or turbulent in origin; Smyth et al. 2013; Thorpe et al. 2013; Li et al. 2015). Nevertheless, in the context of observational oceanography with its inevitable complications and measurement uncertainties (e.g., measurements of Ri tend to be biased large due to averaging), the association of instability with $\mathrm{Ri} < 1/4$ remains a useful rule of thumb.

In Canada's Fraser River estuary, Geyer and Smith (1987) found that Ri was generally near or slightly greater than 1/4, but rarely less, even though instabilities and turbulence were clearly present. They interpreted this to mean that instability begins on the rare occasions when Ri drops below 1/4. The effect of the resulting turbulence is to smooth the velocity and density profiles such that Ri is increased, eventually exceeding the critical value at which point turbulence subsides. This idea was developed further by Thorpe and Liu (2009), who coined the term "marginal instability," and in a sequence of observations of the Pacific equatorial undercurrent (EUC; Smyth and Moum 2013; Smyth et al. 2013, 2017; Pham et al. 2017). Note that "marginal," in this context, does not mean that Ri remains *close* to 1/4, but only that it fluctuates about a central value near 1/4. Fluctuations typically have amplitude near a factor of 2 (e.g., Fig. 2 below).

MI appears to be related to two atmospheric phenomena: global intermittency (Mahrt 2014) and z-less turbulence (section 3c below). Smyth et al. (2019) showed that MI is an example of *self-organized criticality*, a recent paradigm in physics that describes many episodic geophysical phenomena such as landslides, earthquakes and solar flares (e.g., Aschwanden 2014).

a. *Mixing efficiency in MI*

I now argue that if, as in the MI state, Ri fluctuates around a constant value, then so does R_f. Recall that R_f is, by definition, the ratio $\mathrm{Ri}/\mathrm{Pr}_t$. It is often suggested that Pr_t is itself a function of Ri, in which case so is R_f (Table 1, and references therein). The Reynolds hypothesis suggests that, when Ri is small, Pr_t is near unity, implying that R_f is similar in value to Ri. Increasing Ri tends to increase Pr_t. [One way to understand this is to note that adding stratification adds the potential for gravity waves, which transport momentum but not scalars (Sutherland 2010).] We should therefore expect R_f (and Γ) to be somewhat smaller than Ri.

To make this prediction quantitative, we need a specific estimate for Pr_t. A compilation of data from numerous observational and LES studies (Esau and Grachev 2007) provides an empirical parameterization: $\mathrm{Pr}_t = 0.8 + 3.0\mathrm{Ri}$. For Ri = 1/4, this gives $\mathrm{Pr}_t = 1.55$ and $R_f = 0.16$, or $\Gamma = 0.19$. Alternative parameterizations summarized in Table 1 all give Γ values within 40% of 0.2 and well within the scatter of the observational estimates (section 1b).

b. *Ubiquity of MI*

The MI state is commonly observed in the equatorial cold tongues of the eastern Pacific and Atlantic oceans, where diurnally varying "deep cycle" turbulence exchanges heat between the sun-warmed surface layer and

TABLE 2. Observations of sheared, stratified turbulence with Ri near 1/4. Labels refer to Fig. 1.

Label	Locale	Shear forcing	Reference
P	Eastern Pacific EUC	Wind	Smyth and Moum (2013)
A	Eastern Atlantic EUC	Wind	Wenegrat and McPhaden (2015)
G	German Bight	Wind	Schultze et al. (2020)
K	Kuroshio	Wind/topography	Chang et al. (2016)
M	Mediterranean outflow	Gravity	Nash et al. (2012)
H	Exchange flow, Hamilton Harbor	Gravity	Lawrence et al. (2004)
F	Salt-wedge estuary, Fraser River	Gravity	Geyer and Smith (1987)
Col	Columbia River plume	Gravity	Kilcher et al. (2012)
Con	Connecticut River estuary	Gravity	Geyer et al. (2010)
R	Romanche Fracture Zone	Tidal	Van Haren et al. (2014)
B	Benguela Current	Baroclinicity	Peng et al. (2020)
HK	Hong Kong International Airport	Large-scale waves	Chan (2008)

the cold ocean interior (Gregg et al. 1985; Moum and Caldwell 1985; Smyth and Moum 2013; Moum et al. 2013; Smyth et al. 2013; Wenegrat and McPhaden 2015; Pham et al. 2017). The mean shear is forced by the trade winds while the stratification is maintained against diffusion by the combination of solar heating from above and Coriolis-driven upwelling of cold water from below. Although the corresponding region of strong heat uptake in the eastern equatorial Atlantic is smaller, it shares with the Pacific the properties of deep-cycle turbulence (Hummels et al. 2013) and MI (Wenegrat and McPhaden 2015).

Other examples are listed in Table 2 and shown on Fig. 1. The vanishing of the Coriolis effect (either at the equator or in estuaries where the scale is small) makes MI easier to observe, but it is evidently not essential. In summer 2014, Storm Bertha passed over the North Sea, setting up sheared turbulence in which Ri in the thermocline remained close to 1/4 over three distinct intervals, each lasting several hours (Schultze et al. 2020).

In the cases listed so far, sheared currents were forced primarily by wind, but gravity currents also produce MI layers. These have been observed in the Mediterranean Outflow (Nash et al. 2012), the exchange flow between Hamilton Harbor and Lake Ontario (Lawrence et al. 2004), the Fraser river estuary as discussed above, and other river regimes (e.g., Kilcher et al. 2012; Geyer et al. 2010). Tidal flow in the Romanche Fracture Zone produces spectacular trains of KH billows in which Ri varies around ~1/4 (Van Haren et al. 2014), as does flow of the Kuroshio current over a seamount (Chang et al. 2016). In the Benguela Current, a submesoscale filament developed strong thermal wind shear with Ri ~ 1/4 and corresponding strong turbulence (Peng et al. 2020) similar to what we see at the equator. Finally, MI is not observed in the ocean only. Measurements of Ri over Hong Kong International Airport remained near 1/4 at heights and times when pilots reported turbulence, likely forced by large-scale gravity waves (Chan 2008).

Having established the geographical pervasiveness of MI, I now assess its temporal persistence over seasonal and ENSO cycles in the eastern equatorial Pacific. The probability distributions of $\log_{10}$ Ri shown in Fig. 2 were derived from 20 years of measurements made at the Tropical Atmosphere Ocean (TAO) mooring at 0°, 140°W. The peak near Ri = 1/4 is evident despite the use of daily averaged currents and temperature (Pham et al. 2017). Over the seasonal cycle, turbulence is weakest during boreal spring (Fig. 2a, green). Episodes of low (high) Ri are less (more) frequent during that season, but the peak at Ri = 1/4 remains clear.

Over the ENSO cycle, changes are greater. In La Niña conditions (defined by Niño-3.4 index $E_{34} < -1$; Trenberth and Stepaniak 2001), the peak is more pronounced. During El Niño ($E_{34} > 1$), the distribution is spread toward much higher values of Ri, but the peak near 1/4 is still detectable. Over both the seasonal and ENSO cycles, MI is correlated with enhanced turbulence (Smyth and Moum 2013; Warner and Moum 2019).

The ubiquity of MI implies a similar ubiquity of $R_f \approx 0.17$, or $\Gamma = 0.2$. Nevertheless, observations of $R_f \ll 0.17$

FIG. 1. Locations of MI observations listed in Table 2.

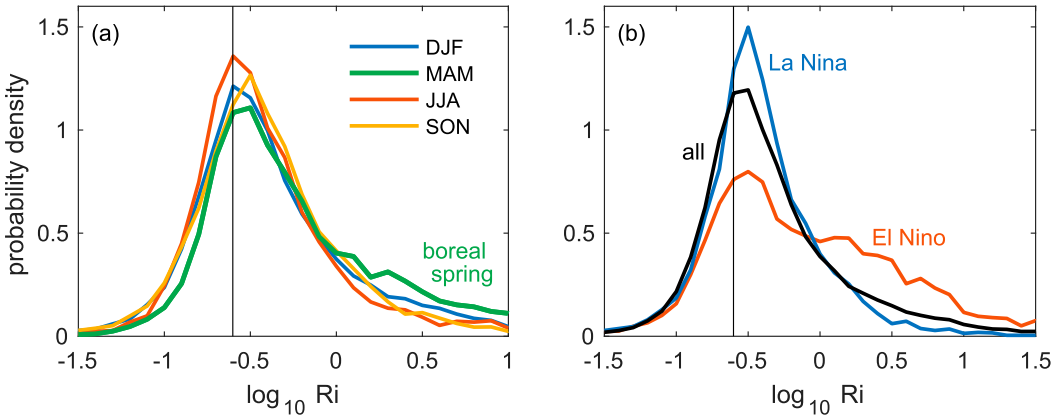

FIG. 2. Probability distribution of $\log_{10}$Ri in the upper equatorial Pacific, subsampled by season and ENSO index. Daily averaged currents and temperature, measured at 0°, 140°W between 1 May 1990 and 26 Nov 2010, are gridded onto 5 m vertical bins and combined to form Ri. Saline stratification is neglected. The deep-cycle layer extends from the daily maximum depth of the mixed layer to 15 m above the EUC core. Data are subsampled by (a) season and (b) Niño-3.4 index. See Pham et al. (2017) for further details.

(or $\Gamma \ll 0.2$) are also common (Monismith et al. 2018). This begs the question–when is ocean turbulence *not* in the MI state? That question is the focus of the following section.

3. When is Γ far from 0.2?

We have seen that Γ should be expected to be near 0.2 (or $R_f \approx 0.16$) in the common case of marginally unstable turbulence. I now turn to circumstances in which MI does not hold and Γ may therefore be far from 0.2. I first describe a "rule of thumb" that predicts when Γ should be especially large or small, then give examples of each extreme.

a. *Scaling* Γ

Consider an eddying motion with length scale ℓ and turnover time ω^{-1}, and assume that all other properties of the eddy are governed by these scales. The specific kinetic energy k is then given by $k \sim \ell^2\omega^2$. Here the tilde indicates proportionality, with the proportionality constant expected to be $O(1)$. (For example, if the eddy is a circular cylinder of radius ℓ in rigid rotation, the constant is 1/4.) The eddy dissipates kinetic energy at a rate

$$\varepsilon \sim k\omega \sim \ell^2\omega^3. \tag{7}$$

Now assume that the fluid is stratified with buoyancy frequency N, but the governing length and time scales are still ℓ and ω^{-1}. Using (7), we can write

$$\frac{\omega}{N} \sim \frac{\varepsilon^{1/3}}{\ell^{2/3}N} \sim \left(\frac{\ell_O}{\ell}\right)^{2/3}, \tag{8}$$

where $\ell_O = \varepsilon^{1/2}/N^{3/2}$ is the Ozmidov scale (Dillon 1982). The condition $\ell \gg \ell_O$ is therefore equivalent to $\omega \ll N$, i.e., the large-scale eddying motion can shed energy by radiating gravity waves. In contrast, eddies with $\ell \ll \ell_O$ spin too rapidly to couple with the gravity wave field and are thus approximately independent of stratification.

Now suppose that a field of similar eddies diffuses the stratification with diffusivity $K_\rho \sim \ell^2\omega$. Combining (1) and (8) gives

$$\Gamma \sim \left(\frac{\omega}{N}\right)^{-2} \sim \left(\frac{\ell}{\ell_O}\right)^{4/3}. \tag{9}$$

This approximation rests on strong assumptions, particularly that stratification does not introduce a new time scale. It should therefore be regarded only as a qualitative indication of the factors governing Γ. There is, however, observational support for this scaling. Ijichi and Hibiya (2018) have measured turbulent overturns at various locations around the Pacific ocean. Using the Thorpe scale ℓ_T as a proxy for ℓ, they find that the relation $\Gamma \sim (\ell_T/\ell_O)^{4/3}$ holds over more than an order of magnitude. Moreover, the constant of proportionality is such that the average value $\ell_T/\ell_O = 0.84$ established by Dillon (1982) corresponds closely to $\Gamma = 0.2$.

These relations suggest that eddies that are large ($\ell \gg \ell_O$) and slow ($\omega \ll N$), and are therefore strongly affected by stratification, should have $\Gamma \gg 0.2$. Conversely, the small, fast eddies that interact only weakly with the stratification have $\Gamma \ll 0.2$. Finally, $\Gamma \approx 0.2$ represents an intermediate case with length and time scales near ℓ_O and N^{-1}, respectively.

b. *Efficient mixing* ($\ell \gg \ell_0$ *and* $\omega \ll N$)

Although mixing is usually enhanced by turbulence, the most efficient mixing appears to take place in

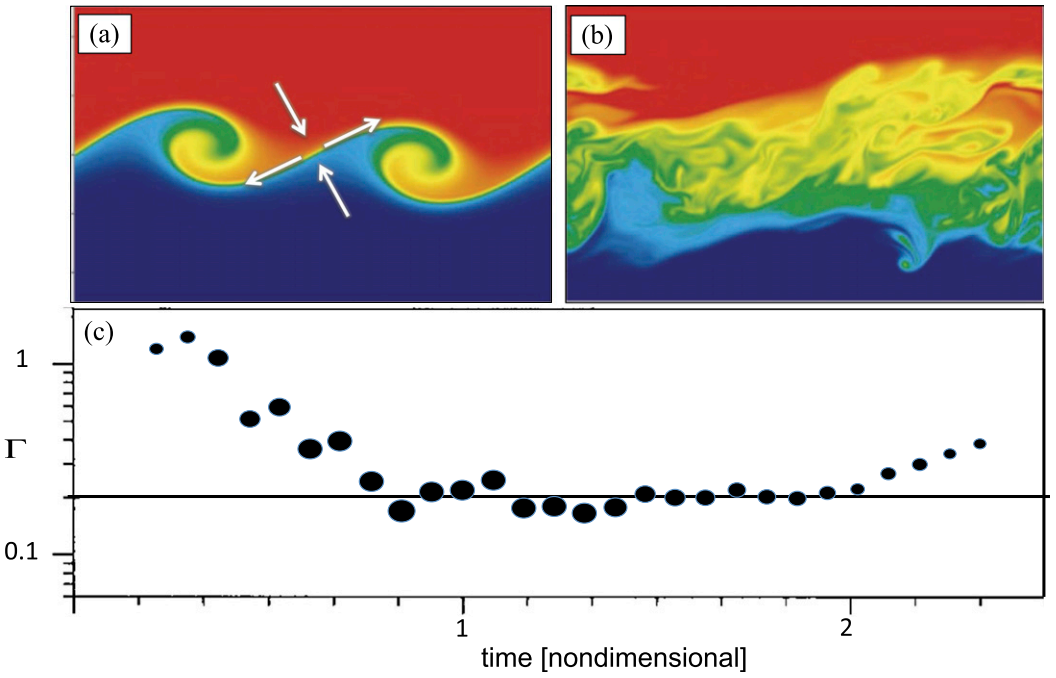

FIG. 3. Transition from efficient, laminar KH billows to less efficient turbulence. The initial condition is a two-layer flow with dense fluid (blue) flowing to the left and buoyant fluid (red) flowing to the right. The molecular Prandtl number Pr = 7. There is no forcing. (a) Buoyancy field in a streamwise–vertical plane early in a simulation showing mature KH billows. Arrows indicate the directions of compressive and extensive principal strains. (b) The same simulation after the transition to turbulence. (c) Γ vs time (scaled by the maximum initial shear) showing the decrease as the flow becomes turbulent. Marker size indicates the magnitude of ε. After Smyth et al. (2001).

slowly evolving coherent structures. For example, Winters et al. (1995) showed that, prior to breaking, KH billows have surprisingly high Γ. Figure 3 shows a direct simulation of a train of KH billows breaking down to form turbulence. Early in the simulation, when the flow consists of large, coherent billows (Fig. 3a), Γ exceeds 0.2 by nearly an order of magnitude (Fig. 3c, left).

Most of this highly efficient mixing occurs in the braids between the KH billows. The flow is still two-dimensional at this stage, and the buoyancy gradient is oriented ideally for compression by the strain field (arrows on Fig. 3a). The resulting sharp buoyancy gradient diffuses rapidly (Corcos and Sherman 1976; Staquet 1995; Smyth 2003), i.e., χ is large. Shear, in contrast, is not enhanced and therefore ε remains small, resulting in large Γ [cf. (6)] as shown on Fig. 3c.

As turbulence develops, Γ decreases. Although the strain is generally stronger in turbulent flow, it lacks persistence, i.e., it changes so rapidly that the buoyancy gradient field is not able to align itself for optimal compression (Fig. 3b; for details see Smyth 1999). In this turbulent state, $\Gamma \approx 0.2$ (Fig. 3c). For an entire KH mixing event, the cumulative, or net, mixing efficiency is sensitive to the Reynolds number but is generally between 0.2 and the higher value characteristic of the preturbulent phase (e.g., Smyth et al. 2001; Mashayek and Peltier 2013).

c. *Inefficient mixing ($\ell \ll \ell_0$ and $\omega \gg N$)*

According to (9), inefficient mixing should be expected when eddies are much smaller than the Ozmidov scale and therefore have frequencies too high to couple to gravity waves. For example, turbulent eddies due to swimming fish can be much smaller than ℓ_O, resulting in $\Gamma \ll 0.2$ (Pujiana et al. 2015).

In the Shih et al. simulations of uniformly stratified shear flow described above (Shih et al. 2000, 2005; Ivey et al. 2008), the maximum eddy size was likely constrained by the periodic boundary conditions rather than by ℓ_O. This effect was explored further by Chung and Matheou (2012). Likewise, the highest-Re_b observations surveyed by Monismith et al. (2018) were generally made close to boundaries. This is not surprising, since the main energy sources for ocean turbulence, namely, wind and tidal flow over topography, act at the boundaries. Because boundary stress can force turbulent eddies of almost arbitrarily small size, regardless of stratification, low mixing efficiency is consistent with (9).

Near a smooth boundary, turbulence can be described by the Monin–Obukhov similarity scaling (Grachev et al. 2015; Scotti and White 2016). Turbulence is assumed to be governed by three parameters only: z, the vertical distance to the boundary; τ, the stress due to the mean wind or current; and J_b, the buoyancy flux at the boundary. Using τ and J_b, one may construct the Monin–Obukhov length scale $\ell_{\rm MO} = (\tau/\rho_0)^{3/2}/(\kappa J_b)$, where $\kappa \approx 0.4$ is the von Kármán constant and ρ_0 is the characteristic density of the fluid. Dimensional consistency then requires that all turbulence statistics be governed by the dimensionless ratio $\zeta = z/\ell_{\rm MO}$. Observations of statically stable boundary layers have yielded empirical expressions for $R_f(\zeta)$, $\Gamma(\zeta)$, and ${\rm Ri}(\zeta)$, e.g., (Kaimal and Finnegan 1994):

$$R_f \approx {\rm Ri} \approx \frac{\zeta}{1+5\zeta} \approx \begin{cases} \zeta\,, & \text{if} \quad \zeta \ll 1 \\ 0.2\,, & \text{if} \quad \zeta \gg 1 \end{cases}$$

$$\Rightarrow \quad \Gamma \approx \frac{\zeta}{1+4\zeta} \approx \begin{cases} \zeta\,, & \text{if } \zeta \ll 1 \\ 0.25\,, & \text{if} \quad \zeta \gg 1 \end{cases}. \qquad (10)$$

Approaching the boundary, ζ becomes $\ll 1$ and Ri, R_f, and Γ all drop linearly to zero. Far from the boundaries, all three parameters approach uniform values. This is the so-called ''z-less'' turbulence regime, where boundary proximity no longer affects the turbulence. The values of Ri, R_f and Γ in the z-less regime are uniform and are similar to those found in the MI turbulence as discussed in section 2.

In the oceanic bottom boundary layer, the buoyancy flux is mostly geothermal and is usually negligible. In that case ℓ_O can itself be used as a scaling variable (Grachev et al. 2015). In observations of the Merrimac River estuary, the turbulent length scale was found to be proportional to ℓ_O when $\ell_O \ll z$ and to z when $\ell_O \gg z$, consistent with the Monin–Obukhov scaling results described above (Scully et al. 2011). Moreover, in the Connecticut River estuary, Holleman et al. (2016) showed that Ri and R_f had approximately uniform values, consistent with MI, except close to the bottom boundary where both parameters approached zero. Both studies confirm a transition from an MI regime to an inefficient, boundary-dominated regime as the boundary is approached.

4. Discussion

This work is part of a community-wide effort to quantify the efficiency of ocean mixing in terms of environmental parameters that are readily measured or computed in numerical models (e.g., Mashayek et al. 2017b). The traditional parameterization $\Gamma = 0.2$, while clearly an oversimplification, has proven remarkably robust. The dual goals of the present paper have been (1) to explain the prevalence of $\Gamma \approx 0.2$ and, (2) to describe some situations in which Γ is significantly different from 0.2.

We have seen that MI is a common property of forced, stratified shear flows in geophysical fluid systems. It represents a quasi-equilibrium between turbulent diffusion and external forcing in which Ri fluctuates around a value close to 1/4 while R_f and Γ fluctuate around 0.17 and 0.2, respectively. MI is found in various geographical settings and driven by various forcings. In the equatorial Pacific cold tongue, where MI has been studied most thoroughly, the phenomenon persists throughout the seasonal cycle and in all phases of the ENSO cycle. This paper has listed many other examples of MI in the ocean, and there is little reason to doubt that more remain to be identified.

A particularly interesting example of MI has been discovered by Salehipour et al. (2018): within the overturning motions of Holmboe waves, small-scale fluctuations are organized so that Ri remains near 1/4. This suggests that the MI dynamic may lurk within other flow structures more complex than the quasi-parallel shear flows I have focused on here. Though MI has been studied primarily in the ocean, it appears to be related to the phenomena called *global intermittency* and *z-less turbulence* in the atmospheric literature (Mahrt 2014). Future exploration of those relationships is likely to be enlightening.

MI depends on a balance between the forcing of the mean shear and whatever buoyancy fluxes act to maintain the mean stratification against turbulent diffusion. Inefficient mixing occurs when turbulence is forced strongly enough to wipe out the stratification, leaving nothing for the turbulence to diffuse, while continuing to dissipate kinetic energy. This happens near boundaries, where forcing is often strong and the mean buoyancy flux is negligible (or of the wrong sign to maintain stability). The largest eddies are then constrained not by stratification but by boundary proximity. An illustrative model of this scenario is provided by the Monin–Obukhov similarity theory (Scotti and White 2016). Whether this inefficient mixing occurs in other geophysical regimes (e.g., over rough topography) remains to be seen.

For the opposite case of high mixing efficiency, the key ingredient is persistent strain, as in our example of preturbulent KH billows. Persistent compressive strain generates sharp scalar gradients, and thus strong scalar diffusion, without dissipating much kinetic energy. We should expect to find this characteristic wherever there are large, slow eddies with vertical scales bigger than the Ozmidov scale. Although this flow state mixes efficiently,

the actual rate of mixing need not be large. Mixing may, however, be long lasting (Smyth et al. 2007; Salehipour et al. 2016). Mashayek et al. (2017a) have argued that the optimal state for mixing, a compromise between turbulence strength and mixing efficiency, occurs in the intermediate state where $\ell_T \sim \ell_O$.

To summarize, in the ocean, we should expect to find low-efficiency layers adjacent to both the upper and lower boundaries. Outside those layers we should expect marginally unstable turbulence with Γ fluctuating around 0.2, punctuated by highly efficient, long-lasting coherent structures. This behavior could extend through much of the ocean, since interior mixing seems to be driven by shear instability of breaking gravity waves (Smyth and Moum 2012), but that remains to be determined. Transitional regimes between MI and stronger but less efficient boundary layer turbulence are an important focus for future investigation as they likely determine the total rate of mixing.

Acknowledgments. This paper has benefited from conversations with Takashi Ijichi, who pointed me to (9), and from critical readings by Jim Moum, Tom Rippeth, Jacob Wenegrat, and an anonymous reviewer. Many thanks to Larissa Schultze, Lucas Merckelbach, Jeffrey Carpenter, Jen-Ping Peng, Peter Holtermann, and Lars Umlauf for sharing results prior to publication. Mooring data were acquired from web archives provided by the TAO Project Office of NOAA/PMEL: https://www.pmel.noaa.gov/tao/drupal/disdel/. This work was supported by the U.S. National Science Foundation under Grants OCE-1355768, OCE-1830071, and OCE-1851520.

REFERENCES

Arya, S. P. S., 1972: The critical condition for the maintenance of turbulence in stratified flows. *Quart. J. Roy. Meteor. Soc.*, **98**, 264–273, https://doi.org/10.1002/qj.49709841603.

Aschwanden, M., 2014: A macroscopic description of a generalized self-organized criticality system: Astrophysical applications. *Astrophys. J.*, **782**, 54, https://doi.org/10.1088/0004-637X/782/1/54.

Bouffard, D., and L. Boegman, 2013: A diapycnal diffusivity model for stratified environmental flows. *Dyn. Atmos. Oceans*, **61-62**, 14–34, https://doi.org/10.1016/j.dynatmoce.2013.02.002.

Boussinesq, J., 1903: *Théorie Analytique de la Chaleur*. Gauthier-Villars, 625 pp.

Britter, R., 1974: An experiment on turbulence in a density-stratified fluid. Ph.D. thesis, Monash University, https://doi.org/10.4225/03/5989249969723.

Chan, P., 2008: Determination of Richardson number profile from remote sensing data and its aviation application. *Earth Environ. Sci.*, **1**, 012043, https://doi.org/10.1088/1755-1307/1/1/012043.

Chang, M.-H., S.-Y. Jheng, and R.-C. Lien, 2016: Trains of large Kelvin-Helmholtz billows observed in the Kuroshio above a seamount. *Geophys. Res. Lett.*, **43**, 8654–8661, https://doi.org/10.1002/2016GL069462.

Chung, D., and G. Matheou, 2012: Direct numerical simulation of stationary homogeneous stratified sheared turbulence. *J. Fluid Mech.*, **696**, 434–467, https://doi.org/10.1017/jfm.2012.59.

Corcos, G., and F. Sherman, 1976: Vorticity concentration and the dynamics of unstable free shear layers. *J. Fluid Mech.*, **73**, 241–264, https://doi.org/10.1017/S0022112076001365.

Dillon, T., 1982: Vertical overturns: A comparison of Thorpe and Ozmidov length scales. *J. Geophys. Res.*, **87**, 9601–9613, https://doi.org/10.1029/JC087iC12p09601.

Ellison, T. H., 1957: Turbulent transport of heat and momentum from an infinite rough plane. *J. Fluid Mech.*, **2**, 456–466, https://doi.org/10.1017/S0022112057000269.

Esau, I., and A. Grachev, 2007: Turbulent Prandtl number in stably stratified atmospheric boundary layer: Intercomparison between LES and SHEBA data. *e-WindEng*, **5**, 1–17.

Geyer, W., and J. Smith, 1987: Shear instability in a highly stratified estuary. *J. Phys. Oceanogr.*, **17**, 1668–1679, https://doi.org/10.1175/1520-0485(1987)017<1668:SIIAHS>2.0.CO;2.

——, A. Lavery, M. Scully, and J. Trowbridge, 2010: Mixing by shear instability at high Reynolds number. *Geophys. Res. Lett.*, **37**, L22607, https://doi.org/10.1029/2010gl045272.

Grachev, A. A., E. L. Andreas, C. W. Fairall, P. S. Guest, and P. O. G. Persson, 2015: Similarity theory based on the Dougherty-Ozmidov length scale. *Quart. J. Roy. Meteor. Soc.*, **141**, 1845–1856, https://doi.org/10.1002/qj.2488.

Gregg, M., H. Peters, J. Wesson, N. Oakey, and T. Shay, 1985: Intensive measurements of turbulence and shear in the equatorial undercurrent. *Nature*, **318**, 140–144, https://doi.org/10.1038/318140a0.

——, E. D'Asaro, J. Riley, and E. Kunze, 2018: Mixing efficiency in the ocean. *Annu. Rev. Mar. Sci.*, **10**, 443–473, https://doi.org/10.1146/annurev-marine-121916-063643.

Holleman, R., W. Geyer, and D. Ralston, 2016: Stratified turbulence and mixing efficiency in a salt wedge estuary. *J. Phys. Oceanogr.*, **46**, 1769–1783, https://doi.org/10.1175/JPO-D-15-0193.1.

Howard, L., 1961: Note on a paper of John W. Miles. *J. Fluid Mech.*, **10**, 509–512, https://doi.org/10.1017/S0022112061000317.

Hummels, R., M. Dengler, and B. Bourlès, 2013: Seasonal and regional variability of upper ocean diapycnal heat flux in the Atlantic cold tongue. *Prog. Oceanogr.*, **111**, 52–74, https://doi.org/10.1016/j.pocean.2012.11.001.

Ijichi, T., and T. Hibiya, 2018: Observed variations in turbulent mixing efficiency in the deep ocean. *J. Phys. Oceanogr.*, **48**, 1815–1830, https://doi.org/10.1175/JPO-D-17-0275.1.

Ivey, G., K. Winters, and J. Koseff, 2008: Density stratification, turbulence, but how much mixing? *Annu. Rev. Fluid Mech.*, **40**, 169–184, https://doi.org/10.1146/annurev.fluid.39.050905.110314.

Kaimal, J., and J. Finnegan, 1994: *Atmospheric Boundary Layer Flows: Their Structure and Measurements*. Oxford University Press, 289 pp.

Katul, G. G., A. Porporato, S. Shah, and E. Bou-Zeid, 2014: Two phenomenological constants explain similarity laws in stably stratified turbulence. *Phys. Rev. E*, **89**, 023007, https://doi.org/10.1103/PhysRevE.89.023007.

Kilcher, L. F., J. D. Nash, and J. N. Moum, 2012: The role of turbulence stress divergence in decelerating a river plume. *J. Geophys. Res.*, **117**, C05032, https://doi.org/10.1029/2011JC007398.

Lawrence, G., R. Pieters, L. Zaremba, E. Tedford, L. Gu, S. Greco, and P. Hamblin, 2004: Summer exchange between Hamilton Harbour and Lake Ontario. *Deep-Sea Res.*, **51**, 475–487, https://doi.org/10.1016/J.DSR2.2003.09.002.

Ledwell, J., K. Polzin, L. St. Laurent, R. Schmitt, and J. Toole, 2000: Evidence for enhanced mixing over rough topography in the abyssal ocean. *Nature*, **403**, 179–182, https://doi.org/10.1038/35003164.

Ledwell, J. R., A. J. Watson, and C. S. Law, 1998: Mixing of a tracer in the pycnocline. *J. Geophys. Res.*, **103**, 21 499–21 529, https://doi.org/10.1029/98JC01738.

——, T. F. Duda, M. A. Sundermeyer, and H. E. Seim, 2004: Mixing in a coastal environment: 1. A view from dye dispersion. *J. Geophys. Res.*, **109**, C10013, https://doi.org/10.1029/2003JC002194.

——, L. C. St. Laurent, J. B. Girton, and J. M. Toole, 2011: Diapycnal mixing in the Antarctic Circumpolar Current. *J. Phys. Oceanogr.*, **41**, 241–246, https://doi.org/10.1175/2010JPO4557.1.

Li, L., W. D. Smyth, and S. A. Thorpe, 2015: Destabilization of a stratified shear layer by ambient turbulence. *J. Fluid Mech.*, **771**, 1–15, https://doi.org/10.1017/jfm.2015.150.

Mahrt, L., 2014: Stably stratified atmospheric boundary layers. *Annu. Rev. Fluid Mech.*, **46**, 23–45, https://doi.org/10.1146/annurev-fluid-010313-141354.

Mashayek, A., and W. R. Peltier, 2013: Shear-induced mixing in geophysical flows: Does the route to turbulence matter to its efficiency? *J. Fluid Mech.*, **725**, 216–261, https://doi.org/10.1017/jfm.2013.176.

——, C. P. Caulfield, and W. R. Peltier, 2017a: Role of overturns in optimal mixing in stratified mixing layers. *J. Fluid Mech.*, **826**, 522–552, https://doi.org/10.1017/jfm.2017.374.

——, H. Salehipour, D. Bouffard, C. P. Caulfield, R. Ferrari, M. Nikurashin, W. R. Peltier, and W. D. Smyth, 2017b: Efficiency of turbulent mixing in the abyssal ocean circulation. *Geophys. Res. Lett.*, **44**, 6296–6306, https://doi.org/10.1002/2016GL072452.

Mellor, G. L., and T. Yamada, 1974: A hierarchy of turbulence closure models for planetary boundary layers. *J. Atmos. Sci.*, **31**, 1791–1806, https://doi.org/10.1175/1520-0469(1974)031<1791:AHOTCM>2.0.CO;2.

Miles, J., 1961: On the stability of heterogeneous shear flows. *J. Fluid Mech.*, **10**, 496–508, https://doi.org/10.1017/S0022112061000305.

Monismith, S., J. Koseff, and B. White, 2018: Mixing efficiency in the presence of stratification: When is it constant? *Geophys. Res. Lett.*, **45**, 5627–5634, https://doi.org/10.1029/2018GL077229.

Moum, J., 1996: Efficiency of mixing in the main thermocline. *J. Geophys. Res.*, **101**, 12 057–12 069, https://doi.org/10.1029/96JC00508.

——, and D. Caldwell, 1985: Local influences on shear flow turbulence in the equatorial ocean. *Science*, **230**, 315–316, https://doi.org/10.1126/science.230.4723.315.

——, A. Perlin, J. Nash, and M. McPhaden, 2013: Ocean mixing controls seasonal sea surface cooling in the equatorial Pacific cold tongue. *Nature*, **500**, 64–67, https://doi.org/10.1038/nature12363.

Nash, J., H. Peters, S. Kelly, J. L. Pelegrí, M. Emelianov, and M. Gasser, 2012: Turbulence and high-frequency variability in a deep gravity current outflow. *Geophys. Res. Lett.*, **39**, L18611, https://doi.org/10.1029/2012GL052899.

Oakey, N., 1982: Determination of the rate of dissipation of turbulent energy from simultaneous temperature and velocity shear microstructure measurements. *J. Phys. Oceanogr.*, **12**, 256–271, https://doi.org/10.1175/1520-0485(1982)012<0256:DOTROD>2.0.CO;2.

——, 1985: Statistics of mixing parameters in the upper ocean during JASIN phase 2. *J. Phys. Oceanogr.*, **15**, 1662–1675, https://doi.org/10.1175/1520-0485(1985)015<1662:SOMPIT>2.0.CO;2.

Osborn, T. R., 1980: Estimates of the local rate of vertical diffusion from dissipation measurements. *J. Phys. Oceanogr.*, **10**, 83–89, https://doi.org/10.1175/1520-0485(1980)010<0083:EOTLRO>2.0.CO;2.

——, and C. S. Cox, 1972: Oceanic fine structure. *Geophys. Fluid Dyn.*, **3**, 321–345, https://doi.org/10.1080/03091927208236085.

Peng, J.-P.., P. Holtermann, and L. Umlauf, 2020: Frontal instability and energy dissipation in a submesoscale upwelling filament. *J. Phys. Oceanogr.*, **50**, 2017–2035, https://doi.org/10.1175/JPO-D-19-0270.1.

Perlin, A., and J. Moum, 2012: Comparison of thermal dissipation rate estimates from moored and profiling instruments at the equator. *J. Atmos. Oceanic Technol.*, **29**, 1347–1362, https://doi.org/10.1175/JTECH-D-12-00019.1.

Pham, H., W. Smyth, S. Sarkar, and J. Moum, 2017: Seasonality of deep cycle turbulence in the eastern equatorial Pacific. *J. Phys. Oceanogr.*, **47**, 2189–2209, https://doi.org/10.1175/JPO-D-17-0008.1.

Pope, S., 2000: *Turbulent Flows*. Cambridge University Press, 771 pp.

Pujiana, K., J. N. Moum, W. D. Smyth, and S. J. Warner, 2015: Distinguishing ichthyogenic turbulence from geophysical turbulence. *J. Geophys. Res. Oceans*, **120**, 3792–3804, https://doi.org/10.1002/2014JC010659.

Ruddick, B., D. Walsh, and N. Oakey, 1997: Variations in apparent mixing efficiency in the North Atlantic central water. *J. Phys. Oceanogr.*, **27**, 2589–2605, https://doi.org/10.1175/1520-0485(1997)027<2589:VIAMEI>2.0.CO;2.

Salehipour, H., W. R. Peltier, C. B. Whalen, and J. A. MacKinnon, 2016: A new characterization of the turbulent diapycnal diffusivities of mass and momentum in the ocean. *Geophys. Res. Lett.*, **43**, 3370–3379, https://doi.org/10.1002/2016GL068184.

——, ——, and C. P. Caulfield, 2018: Self-organized criticality of turbulence in stratified mixing layers. *J. Fluid Mech.*, **856**, 228–256, https://doi.org/10.1017/jfm.2018.695.

Schultze, L. K. P., L. M. Merckelbach, and J. R. Carpenter, 2020: Storm-induced turbulence alters shelf sea vertical fluxes. *Limnol. Oceanogr. Lett.*, **5**, 264–270, https://doi.org/10.1002/lol2.10139.

Scotti, A., and B. White, 2016: The mixing efficiency of stratified turbulent boundary layers. *J. Phys. Oceanogr.*, **46**, 3181–3191, https://doi.org/10.1175/JPO-D-16-0095.1.

Scully, M. E., W. R. Geyer, and J. H. Trowbridge, 2011: The influence of stratified and nonlocal turbulent production on estuarine turbulence: An assessment of turbulence closure with field observations. *J. Phys. Oceanogr.*, **41**, 166–185, https://doi.org/10.1175/2010JPO4470.1.

Shih, L., J. Koseff, J. Ferziger, and C. Rehmann, 2000: Scaling and parameterization of stratified homogeneous turbulent shear flow. *J. Fluid Mech.*, **412**, 1–20, https://doi.org/10.1017/S0022112000008405.

——, ——, G. Ivey, and J. Ferziger, 2005: Parameterization of turbulent fluxes and scales using homogeneous sheared stably stratified turbulence simulations. *J. Fluid Mech.*, **525**, 193–214, https://doi.org/10.1017/S0022112004002587.

Smyth, W., 1999: Dissipation range geometry and scalar spectra in sheared, stratified turbulence. *J. Fluid Mech.*, **401**, 209–242, https://doi.org/10.1017/S0022112099006734.

——, 2003: Secondary Kelvin-Helmholtz instability in a weakly stratified shear flow. *J. Fluid Mech.*, **497**, 67–98, https://doi.org/10.1017/S0022112003006591.

——, and J. Moum, 2012: Ocean mixing by Kelvin-Helmholtz instability. *Oceanography*, **25**, 140–149, https://doi.org/10.5670/oceanog.2012.49.

——, and ——, 2013: Marginal instability and deep cycle turbulence in the eastern equatorial Pacific Ocean. *Geophys. Res. Lett.*, **40**, 6181–6185, https://doi.org/10.1002/2013GL058403.

——, and J. R. Carpenter, 2019: *Instability in Geophysical Flows*. Cambridge University Press, 338 pp.

——, J. Moum, and D. Caldwell, 2001: The efficiency of mixing in turbulent patches: Inferences from direct simulations and microstructure observations. *J. Phys. Oceanogr.*, **31**, 1969–1992, https://doi.org/10.1175/1520-0485(2001)031<1969:TEOMIT>2.0.CO;2.

——, J. Carpenter, and G. Lawrence, 2007: Mixing in symmetric Holmboe waves. *J. Phys. Oceanogr.*, **37**, 1566–1583, https://doi.org/10.1175/JPO3037.1.

——, J. Moum, L. Li, and S. Thorpe, 2013: Diurnal shear instability, the descent of the surface shear layer, and the deep cycle of equatorial turbulence. *J. Phys. Oceanogr.*, **43**, 2432–2455, https://doi.org/10.1175/JPO-D-13-089.1.

——, J. Nash, and J. Moum, 2019: Self-organized criticality in geophysical turbulence. *Nature Sci. Rep.*, **9**, 3747, https://doi.org/10.1038/S41598-019-39869-W.

——, H. T. Pham, J. N. Moum, and S. Sarkar, 2017: Pulsating turbulence in a marginally unstable stratified shear flow. *J. Fluid Mech.*, **822**, 327–341, https://doi.org/10.1017/jfm.2017.283.

Staquet, C., 1995: Two-dimensional secondary instabilities in a strongly stratified shear layer. *J. Fluid Mech.*, **296**, 73–126, https://doi.org/10.1017/S0022112095002072.

Sutherland, B., 2010: *Internal Gravity Waves*. Cambridge University Press, 377 pp.

Thorpe, S., and Z. Liu, 2009: Marginal instability? *J. Phys. Oceanogr.*, **39**, 2373–2381, https://doi.org/10.1175/2009JPO4153.1.

——, W. Smyth, and L. Li, 2013: The effect of small viscosity and diffusivity on the marginal stability of stably stratified shear flows. *J. Fluid Mech.*, **731**, 461–476, https://doi.org/10.1017/jfm.2013.378.

Trenberth, K. E., and D. P. Stepaniak, 2001: Indices of El Niño evolution. *J. Climate*, **14**, 1697–1701, https://doi.org/10.1175/1520-0442(2001)014<1697:LIOENO>2.0.CO;2.

Van Haren, H., L. Gostiaux, E. Morozov, and R. Tarakanov, 2014: Extremely long Kelvin-Helmholtz billow trains in the Romanche Fracture Zone. *Geophys. Res. Lett.*, **41**, 8445–8451, https://doi.org/10.1002/2014GL062421.

Venayagamoorthy, S., and D. Stretch, 2010: On the turbulent Prandtl number in homogeneous stably stratified turbulence. *J. Fluid Mech.*, **644**, 359–369, https://doi.org/10.1017/S002211200999293X.

Warner, S. J., and J. N. Moum, 2019: Feedback of mixing to ENSO phase change. *Geophys. Res. Lett.*, **46**, 13 920–13 927, https://doi.org/10.1029/2019GL085415.

Wenegrat, J., and M. McPhaden, 2015: Dynamics of the surface layer diurnal cycle in the equatorial Atlantic ocean (0°, 23°W). *J. Geophys. Res. Oceans*, **120**, 563–581, https://doi.org/10.1002/2014JC010504.

Winters, K., P. Lombard, J. Riley, and E. A. D'Asaro, 1995: Available potential energy and mixing in density-stratified fluids. *J. Fluid Mech.*, **289**, 115–128, https://doi.org/10.1017/S002211209500125X.